Communication

A Wideband Dual-Polarized Dielectric Magnetoelectric Dipole Antenna

Zhen-Yuan Zhang and Ke-Li Wu

***Abstract*— A new wideband ±45° dual-polarized metal loop dielectric resonator magnetoelectric antenna is proposed in this communication. The antenna consists of two orthogonal dielectric bars that support two orthogonal electric dipoles and two cross interlaced metal semi-loops that are equivalent to two orthogonal magnetic dipoles above the ground. With a legitimate combination of the electric and magnetic dipoles, a unidirectional radiation with low backward radiation and equal E-plane and H-plane radiation patterns can be achieved. The antenna can be made of a monolithic dielectric block with simple installation. To validate the new antenna configuration, a prototype is designed, manufactured, and measured. The prototype antenna using ceramic with the electrical size of $0.33\lambda_o \times 0.33\lambda_o \times 0.21\lambda_o$ demonstrates that an impedance bandwidth of 11.4% ($|S_{11}| < -15$ dB) in the 3.5 GHz frequency band can be achieved with the measured forward/backward ratio of better than 22 dB. The proposed antenna is suitable as antenna element for massive-MIMO array antennas, where a large number of antenna elements need to be installed in a compact space.**

***Index Terms*— Dielectric resonator antennas (DRAs), differential-fed antennas, low backward radiation, magnetoelectric dipole (ME dipole) antenna, ±45° dual-polarized antennas.**

I. Introduction

With the diverse requirements for various communication systems, innovative antenna element forms and configurations have gained a considerable attention in past two decades. In a traditional base station for 3G and 4G systems, the dual-polarized half-wavelength dipole antenna as a basic element in an antenna array is the most prevalent antenna configuration [1], [2]. Half-wavelength dipolelike antennas have many attractive features, including wide bandwidth, broadside and stable radiation patterns, metal-cast manufacturability, and steady mechanical structure. The dual-polarized dipole antenna with ±45° inclination can be readily constructed in a complementary arrangement for base station applications. Since a traditional antenna array only needs to provide a wide angle sector coverage in azimuth direction and a shaped beam in elevation direction, the antenna array usually is 1-D and the size of antenna elements is not very critical. However, for future wireless communication systems, the massive-MIMO (M-MIMO) technology is considered to be a compulsory means to increase spatial multiplexing [3]. 2-D array antennas will be employed for base stations. Clearly, the number of antenna elements will be increased by tens of times as compared to the conventional base station antennas for 4G systems. The greater the number of antenna elements, the higher the spatial multiplexing gain and channel capacity. To confront the forthcoming challenges in size and cost reduction for array antennas, new antenna configurations that are more suitable for M-MIMO array antennas need to be developed. A compact antenna element allows potential reduction of the overall array size and alleviates the pressure on mutual coupling among the antenna elements [4]. Therefore, a compact yet wideband dual-polarized antenna element that radiates broadside with a high forward/backward (F/B) radiation ratio is always desirable. Typically, an F/B ratio of greater than 18 dB is required for reducing the interference from the backside and the neighboring array antennas. F/B ratio is usually defined as the ratio of the antenna gains in the forward and backward directions within the angle of ±30°.

By intuition, dielectric resonator antenna (DRA) is a good candidate for reducing the antenna size. To achieve a wideband or multiband characteristic of a DRA, a popular method is to excite multiple resonant modes in a dielectric resonator in the frequency band of interest [5]–[10]. Another common method to broaden the impedance bandwidth is to use a coupled feeding structure [11]–[14]. However, a poor F/B ratio is always a weakness for most of the DRAs.

To improve the F/B ratio for a broadside antenna element while achieving a wide impedance bandwidth, the antenna configurations with the built-in feature of low backward radiation have drawn a great deal of attention in recent years. A wideband magnetoelectric dipole (ME dipole) antenna with a low cross polarization and low backward radiation is proposed in [15]. The pioneer work is followed by a number of variations including dual-polarized ME dipole antennas [16]–[21], a waveguide-based dual-polarized ME dipole antenna [21], and a differentially fed dual-polarized ME dipole antenna with improved port-to-port isolation and bandwidth [20]. However, the dimensions of these antennas are typically on the order of $0.6\lambda_o \times 0.6\lambda_o \times 0.25\lambda_o$, where λ_o is the free-space wavelength at the center frequency, which is too large for M-MIMO array antennas. A linearly polarized broadside DRA with a low F/B ratio and its extension to a circularly polarized antenna are reported in [22]. Since the ground plane of the antenna acts as an electric dipole, it is difficult to use in an M-MIMO array antenna with a large ground plane.

In this communication, a new type of wideband ±45° dual-polarized metal loop dielectric resonator ME (MLDR-ME) dipole antenna with low backward radiation and symmetrical E-plane and H-plane radiation patterns for a broadside array is proposed. This differentially fed MLDR-ME dipole antenna is comprised of two perpendicular metal semi-loop radiators and a cross-shaped dielectric resonator. The metal semi-loops serve as the feeding structure for the two orthogonal modes in the dielectric resonator, as well as two magnetic dipole antennas, whereas each of the resonant modes in the dielectric resonator creates an electric dipole. With appropriate balance in magnitude, the backward radiation of the two types of dipoles can be canceled in a great extent while their forward radiation is superposed in phase.

To validate the proposed antenna, a prototype with ceramic material of dielectric constant 12 is designed and fabricated. The electrical dimension of the prototyped antenna is $0.33\lambda o \times 0.33\lambda o \times 0.21\lambda o$, where λo is the wavelength at 3.5 GHz. The measured F/B ratios of the prototype antenna are better than 22 dB with the ground plane size of $1.15\lambda o \times 1.15\lambda o$. It is worth mentioning that the measured maximum and minimum radiation efficiencies of the prototype antenna over the operating frequency band are better than 96% and

Manuscript received October 31, 2017; revised June 2, 2018; accepted June 22, 2018. Date of publication July 26, 2018; date of current version October 4, 2018. This work was supported by the Postgraduate scholarship of The Chinese University of Hong Kong. *(Corresponding author: Ke-Li Wu.)*

The authors are with the Department of Electronic Engineering, The Chinese University of Hong Kong, Hong Kong (e-mail: zyzhang@ee.cuhk.edu.hk; klwu@cuhk.edu.hk).

Color versions of one or more of the figures in this communication are available online at http://ieeexplore.ieee.org.

Digital Object Identifier 10.1109/TAP.2018.2859914

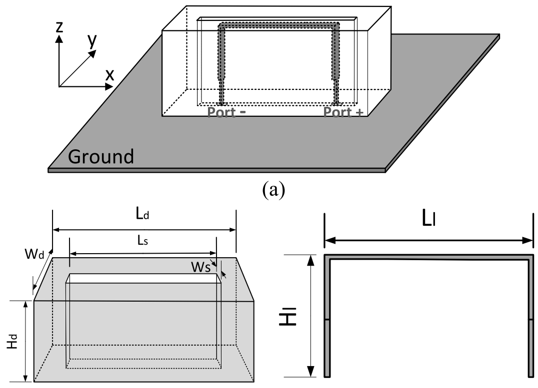

Fig. 1. (a) Configuration of a proposed differentially fed linear-polarized MLDR-ME dipole antenna. (b) Structure of the dielectric resonator. (c) Structure of a metal semi-loop ($L_d = 40$, $W_d = 25$, $H_d = 17$, $L_s = 36$, $W_s = 3.4$, $H_l = 17$, and $L_l = 24.6$, unit: millimeter).

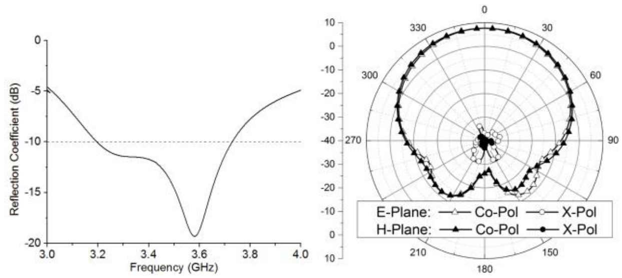

Fig. 2. Simulated characteristics of a linearly polarized MLDR-ME dipole antenna. (a) Reflection coefficient and (b) radiation patterns at 3.5 GHz.

86%, respectively. With the attractive features of a compact size, monoblock structure, wideband, high F/B ratio, and stable radiation patterns in a wide frequency band, the prototype antenna has demonstrated a promising potential for M-MIMO array antenna applications. Detailed features and experimental results will be presented in the following sections.

II. Antenna Configuration and Working Mechanism

A. Linearly Polarized Prototype and Working Mechanism

In this section, the working mechanism of the MLDR-ME dipole antenna will be explained. Since a dual-polarized cross-shaped dielectric resonator is formed by two linearly polarized DRAs, to have a full understanding of the dual-polarized antenna, a linearly polarized MLDR-ME dipole antenna with the relative permittivity of 6.85 is simulated using ANSYS HFSS. Fig. 1 illustrates the configuration of a differentially fed linearly polarized MLDR-ME antenna. The linear antenna consists of a rectangular cylindrical dielectric resonator and a metallic semi-loop, both of which are installed on a square ground plane of size 100 mm^2. The simulated reflection coefficient and the radiation patterns at 3.5 GHz are shown in Fig. 2. As shown in Fig. 2(a), the 10 dB return loss bandwidth spans from 3.2 to 3.7 GHz, which is achieved by an appropriate coupling between the dielectric resonator and the metal semi-loop. It can be seen from Fig. 2(b) that back-lobe cancelation is achieved.

To explain the working mechanism, Fig. 3(a) and (b) shows the electric field distribution on an *xy* plane and an *xz* plane at 3.3 GHz, at which the metal semi-loop resonates with the electric current distribution shown in Fig. 3(c) when "port $^-$" and "port $^+$" are excited with the same magnitude but opposite phases. With the image current induced by the ground plane, the current loop is equivalent

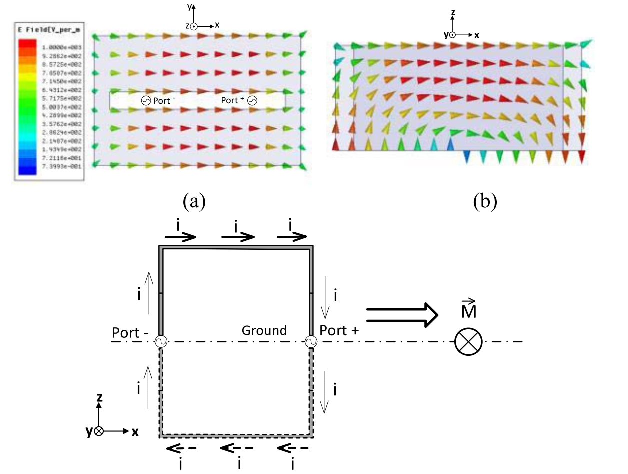

Fig. 3. (a) E-field distribution on an *xy* plane at 3.3 GHz. (b) E-field distribution on an *xz* plane at 3.3 GHz. (c) Current distribution on a semi-loop and its equivalent magnetic dipole when port$^-$ and port$^+$ are excited.

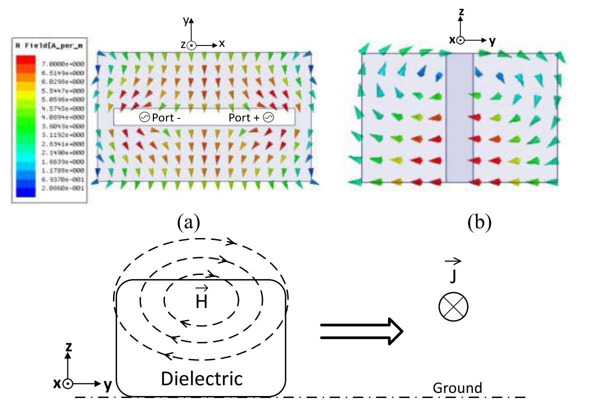

Fig. 4. (a) H-field distribution on an *xy* plane at 3.6 GHz. (b) H-field distribution on a *yz* plane at 3.6 GHz. (c) Sketch of rotational H-field and its equivalent electric dipole when port$^-$ and port$^+$ are excited.

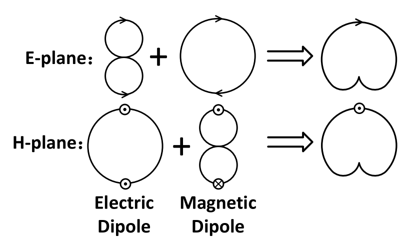

Fig. 5. Superposition of radiation patterns of the electric and the magnetic dipoles.

to a magnetic dipole along the axis of the loop. Fig. 4(a) and (b) depicts the magnetic field distribution inside the dielectric resonator at 3.6 GHz, at which the dielectric resonator is in resonance. Fig. 4(c) sketches the H-field lines in a *yz* cutting plane at the middle of the dielectric resonator, which is equivalent to an electric dipole.

The semi-loop plays two roles: to realize a magnetic dipole and to excite an electric dipole inside the dielectric resonator. The electric and magnetic dipoles are polarized perpendicularly. Therefore, the semi-loop should resonate at the right frequency and provide a good matching to the resonant mode in the dielectric resonator.

As shown in Fig. 5, it is understandable that the electric dipole has an "8-shaped" radiation pattern in the E-plane and an "O-shaped" pattern in the H-plane, whereas the magnetic dipole has an

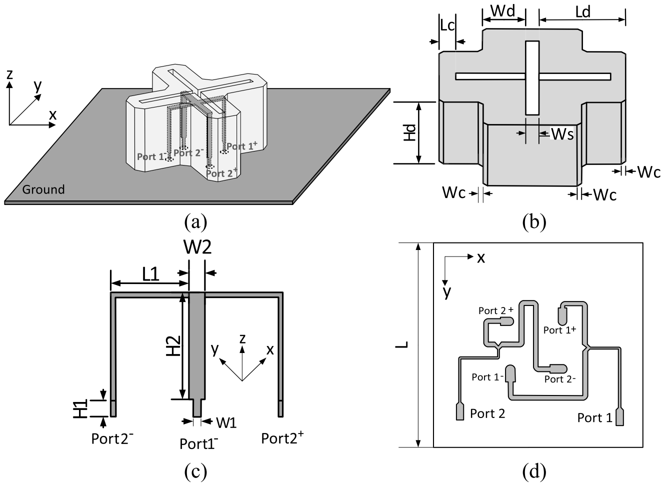

Fig. 6. (a) Configuration of the differential fed ±45° ceramic dual-polarized MLDR-ME dipole antenna. (b) Structure of the dielectric block. (c) Two orthogonal metal loops. (d) Differential feeding networks.

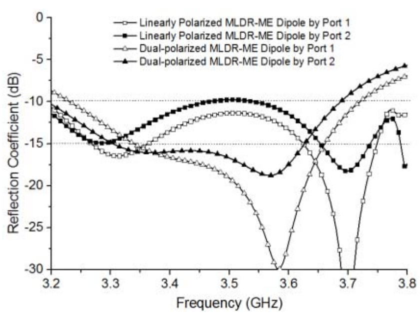

Fig. 7. Simulated reflection coefficients of linearly polarized MLDR-ME antennas and dual-polarized MLDR-ME antenna.

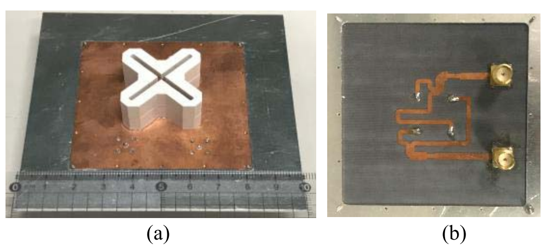

(a) (b)

Fig. 8. (a) Photograph of the differential-fed ±45° dual-polarized MLDR-ME dipole antenna with ceramic material. (b) Photograph of the feeding networks.

"O-shaped" radiation pattern in the E-plane and an "8-shaped" radiation pattern in the H-plane. With an appropriate weighting of the strength of the electric and magnetic dipoles, the backward radiated electric fields from the two dipoles can be canceled each other whereas the forwarded radiated electric fields are superposed in phase, leading to a broadside radiation pattern with low backward radiation [23].

B. Configuration of the Dual-Polarized MLDR-ME Antenna

The detailed configuration of the proposed dual-polarized MLDR-ME antenna is illustrated in Fig. 6(a). The antenna is comprised of two major parts: a cross-shaped dual-metal semi-loop and a cross-shaped dielectric resonator. Assume a finite-ground plane is with the size of $L \times L$. Fig. 6(b) shows the structure of the dielectric block with the length, width, and height of L_d, W_d, and H_d, respectively. Chamfered corners with the size of W_c are provided to protect the corners from breaking. The chamfered corners do not affect the performance of the antenna too much. A monoblock

TABLE I
DIMENSIONS OF THE PROTOTYPE ANTENNA

	L	L_d	W_d	H_d	W_s	W_c
mm	150	16.7	3.95	18	1.6	2
λ_o	1.8	0.19	0.05	0.2	0.02	0.02
	L_c	L_1	W_1	W_2	H_1	H_2
mm	3	7.3	1	1.6	2	12.5
λ_o	0.03	0.09	0.01	0.02	0.02	0.15

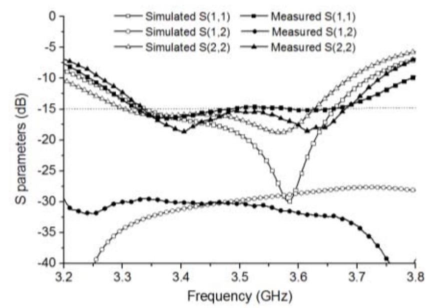

Fig. 9. Simulated and measured S-parameters of the ceramic dual-polarized MLDR-ME dipole antenna.

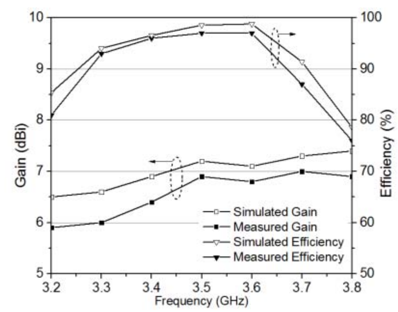

Fig. 10. Simulated and measured gain and efficiency of the ceramic dual-polarized MLDR-ME antenna with port 1 excited and port 2 terminated.

structure with a cross slot is a convenient choice for mass production. The structure of the crossed dual-metal loops and its dimensions are shown in Fig. 6(c). The dual loops serve as the feeding structure to the dielectric resonator dipole antenna as well as two perpendicular magnetic dipoles. The metal structure can be formed by stamping a copper sheet with the thickness of 0.5 mm. The total length of each semi-loop is approximately $0.5\lambda_o$, where λ_o is the wavelength of operating frequency. The height of the semi-loops is a design parameter for impedance matching. The resonance of the semi-loop depends on the size of the dielectric resonator. The two ends of each semi-loop are soldered to a 50 Ω transmission line on the other side of the ground plane, on which four ports, namely, port 1^-, port 1^+, port 2^-, and port 2^+, are defined. As shown in Fig. 6(d), two differential feeding networks are designed to feed the two cross-polarized antennas. By feeding the differential ports of the two perpendicular antennas, two orthogonal modes inside the dielectric resonator can be excited. Ports 1^+–1^- excite the mode with the polarization along +45° direction, while ports 2^+–2^- excite the mode polarized along −45° direction. The cross-shaped semi-loop and dielectric block can be configured simply by duplicating the linearly polarized dipole orthogonally. Fig. 7 shows the reflection coefficients of two linearly polarized MLDR-ME dipole antennas fed by ports 1 and 2, respectively, and the dual-polarized MLDR-ME dipole antenna. It can be seen from Fig. 7 that by duplicating another arm, the operating frequency does not change too much, while the −10 dB impedance bandwidth is shrunk after duplicating the

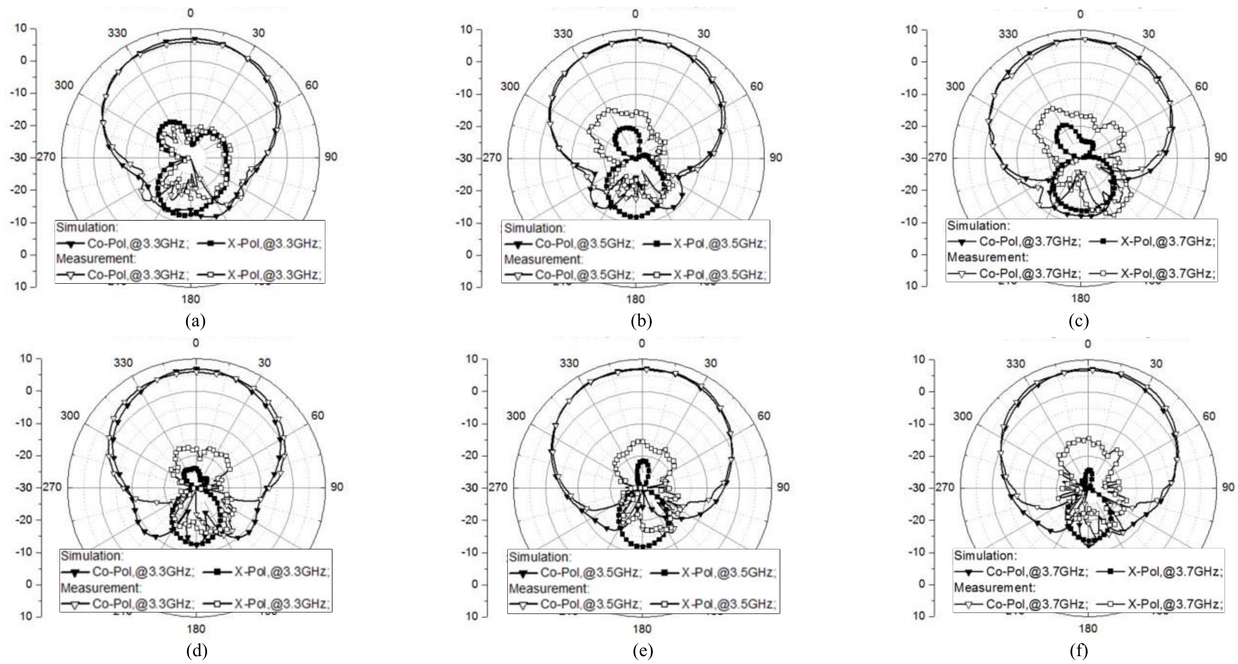

Fig. 11. Simulated and measured radiation patterns of port 1 at 3.3, 3.5, and 3.7 GHz. (a)–(c) E-Plane. (d)–(f) H-Plane.

semi-loop and dielectric block. A fine tuning of the dual-polarized antenna is needed with the help of a parametric study.

C. Design of Differential Feeding Network

The dual-polarized antenna can be treated as a four-port network with port 1^-, port 1^+, port 2^-, and port 2^+, as defined in Fig. 6(d). Due to the symmetry of the antenna structure, the scattering matrix of the four-port antenna can be expressed as

$$S_a = \begin{bmatrix} \Gamma & T_1 & T_2 & T_1 \\ T_1 & \Gamma & T_1 & T_2 \\ T_2 & T_1 & \Gamma & T_1 \\ T_1 & T_2 & T_1 & \Gamma \end{bmatrix} \tag{1}$$

where Γ is the reflection coefficient of each port and T_1 is the mutual coupling between adjacent ports, such as ports 1^- and 2^-, and T_2 is the mutual coupling between the same pair of ports, such as ports 1^- and 1^+. The feeding network splits the power with the same magnitude but opposite phase. With the matched condition, the scattering matrix of each feeding network can be expressed as

$$S_n = \begin{bmatrix} 0 & -\frac{j}{\sqrt{2}}e^{-j\varphi} & \frac{j}{\sqrt{2}}e^{-j\varphi} \\ -\frac{j}{\sqrt{2}}e^{-j\varphi} & -\frac{1}{2}e^{-j2\varphi} & -\frac{1}{2}e^{-j2\varphi} \\ \frac{j}{\sqrt{2}}e^{-j\varphi} & -\frac{1}{2}e^{-j2\varphi} & -\frac{1}{2}e^{-j2\varphi} \end{bmatrix} \tag{2}$$

where φ is the phase shift for the signal traveling between the common port and a differential port. Assume φ_1 and φ_2 are the phase shift for feeding networks 1 and 2, respectively. The scattering matrixes of the two antennas and the two feeding networks can be cascaded with each other. It is straightforward to find that the cascaded scattering matrix can be written as

$$S_d = \begin{bmatrix} (\Gamma - T_2)\, e^{-(j2\varphi_1+\pi)} & 0 \\ 0 & (\Gamma - T_2)\, e^{-(j2\varphi_2+\pi)} \end{bmatrix}. \tag{3}$$

Obviously, a high isolation between the two orthogonal antennas is naturally guaranteed. However, the magnitude of the reflection coefficients depends on the difference between Γ and T_2. In order to match the antenna ports, the antenna has to be optimized to minimize the difference in a wideband sense.

TABLE II
MEASURED 3 dB BEAMWIDTH OF THE PROTOTYPE ANTENNAS

Frequency (GHz)	Ceramic MLDR-ME antenna		
	3-dB beam width		Front-to-Back Ratio
	E-plane	H-plane	
3.3	103°	108°	20 dB
3.5	96°	101°	22 dB
3.7	80°	101°	20 dB

III. PROTOTYPE ANTENNA

To validate the proposed antenna, a ceramic prototype antenna is designed, fabricated, and fully tested. In the design, the operating frequency band is chosen to be in the range of 3.3–3.7 GHz, a popular frequency band for 5G. In the prototype, the ground plane size is 100 mm × 100 mm. All the radiation properties are measured using the SATIMO SG-128 spherical scanner in an in-house ISO17025 accredited laboratory.

Fig. 8(a) shows a photograph of the finished prototype antenna. The permittivity of the ceramic material is 12. The physical dimensions of the fabricated prototype antenna are listed in Table I, and the electrical size is $0.33\lambda_o \times 0.33\lambda_o \times 0.21\lambda_o$, where λ_o is the free-space wavelength at 3.5 GHz, with the feeding networks shown in Fig. 8(b). The simulated and measured S-parameters of the prototype antenna are shown in Fig. 9. The bandwidth of 15 dB return loss spans from 3.3 to 3.7 GHz, within which the isolation between the two ports is better than 30 dB.

The simulated and measured gain and the measured radiation efficiency are superimposed in Fig. 10. It can be seen that the 1 dB gain bandwidth extends from 3.2 to 4 GHz. The measured peak total radiation efficiency of the prototype antenna is better than 96%. Due to the symmetry, only the simulated and measured radiation patterns of port 1 at 3.3, 3.5, and 3.7 GHz are shown in Fig. 11. The simulated and measured peak gain at the broadside direction over the operating

TABLE III

COMPARISON OF THE PROPOSED ANTENNA WITH EXISTING DUAL-POLARIZED ANTENNAS

Ref (Year)		Antenna Dimensions		Ground Sizes		Impedance Bandwidth (GHz) (%)	1-dB Gain Bandwidth (%)	Gain (dBi)	F/B Ratio (dB)
		Physical (mm^3)	**Electrical (λ_o)***	**Physical (mm)**	**Electrical (λ_o)***				
DRAs	[8] (2013)	35.5 × 35.5 × 52	0.29 × 0.29 ×0.42	150 × 150	1.22 × 1.23	2.1 - 2.8, SWR < 2 (14.3%)	~8%	3.7 - 8.4	> 11
	[9] (2017)	31 × 31 × 24.5	0.14 × 0.14 × 0.11 @1.4 GHz / 0.21 × 0.21 × 0.17 @2.0 GHz	Not Available	Not Available	1.365 - 1.425 / 2.0275-2.0525, SWR < 2 (4.3% / 1.2%)	Not Available	3.92 / 2.82	15 / 10
	[13] (2003)	40 × 40 × 20	0.3 × 0.3 × 0.15	200 × 150	1.5 × 1.12	1.98 - 2.26, SWR < 2 (13.1%)	Not Available	5.5	> 10
M-E Dipoles	[17] (2009)	77.7 × 77.7 × 24	0.46 × 0.46 × 0.14	130 × 130 × 24 (with grounded wall)	0.77 × 0.77 × 0.14	1.65 - 2.12, SWR < 2 (25%)	> 25%	~8.2	> 15
	[20] (2009)	64.6 × 64.6 × 28	0.55 × 0.55 × 0.16	150 × 150	1.28 × 1.28	1.72 - 3.4, SWR < 2 (66%)	55%	~9.5	> 25
	[21] (2013)	122 × 122 × 48	0.59 × 0.59 × 0.23	260 × 260	1.26 × 1.26	0.98 - 1.9, SWR < 2 (64%)	40%	6.6 - 9.6	> 20
	[22] (2017)	28 × 28 × 22.4	0.93 × 0.93 × 0.75	No Ground	No Ground	7 – 13.6, SWR < 2 (64%)	> 64%	4.2 - 6.1	> 20
Printed Dipoles	[24] (2017)	76 × 76 × 34.8	0.58 × 0.58 × 0.26	140 × 140 × 6 (with grounded wall)	1.07 × 1.07 × 0.05	1.7 - 2.9, SWR < 1.5 (52%)	> 52%	~8.5	> 25
	[25] (2014)	85 × 85 × 32.5	0.65 × 0.65 × 0.25	150 × 150	1.15 × 1.15	1.7 – 2.9, SWR < 1.5 (52%)	> 52%	7 - 8.6	> 17
This Work	Ceramic (ε_r = 12)	28.7 × 28.7 × 18	0.33 × 0.33 × 0.21	100 × 100	1.15 × 1.15	3.3 - 3.7, SWR < 1.5 (11.4%)	> 11.4%	~7	> 22

*: λ_o is the free-space wavelength at the center frequency.

frequency band is about 7 dBi. The measured 3 dB beamwidth and F/B ratio at 3.3, 3.5, and 3.7 GHz are listed in Table II.

A comparison of antenna performance between the proposed MLDR-ME antenna and other broadside radiation dual-polarized antennas is listed in Table III. With a comparable antenna gain to those of conventional ME dipoles, the electrical dimension of the ceramic MLDR-ME dipole antenna is the smallest. Comparing with the existing dual-polarized DRAs, the F/B ratio of the proposed antenna is improved by more than 10 dB, and the flatness of the antenna gain is significantly improved. Here, the F/B ratio is defined as the ratio of the antenna gains in the forward and backward directions within the angle of $\pm 30°$.

IV. DESIGN GUIDELINE

To investigate a design guideline of the proposed MLDR-ME dipole antenna, a parametric study on the linearly polarized prototype shown in Fig. 1 is conducted. The study shows how the key dimensions affect the matching condition of the antenna. The size of the ground plane is also perturbed in the HFSS model to show that the back-lobe cancelation has nothing to do with the ground size. The estimation of the dimensions of the dielectric block and the metallic loop will be included in the design guidelines.

A. Parametric Study

It can be seen from Fig. 2(a) that there are two resonances within the operational bandwidth. The parametric study is focused on which parameter controls the resonant frequencies. Fig. 12 shows that the upper resonance is largely controlled by the width of the dielectric resonator. Fig. 13 suggests that the lower resonance heavily depends on the total length of the semi-loop. In fact, the total length of the semi-loop is approximately $0.5\lambda_o$ long. Since the lower resonant frequency is mainly controlled by the semi-loop, the length L_t is slightly longer than $0.5\lambda_o$.

EM-simulated reflection coefficients for the antenna prototype with different slot lengths are illustrated in Fig. 14(a). It can be obviously

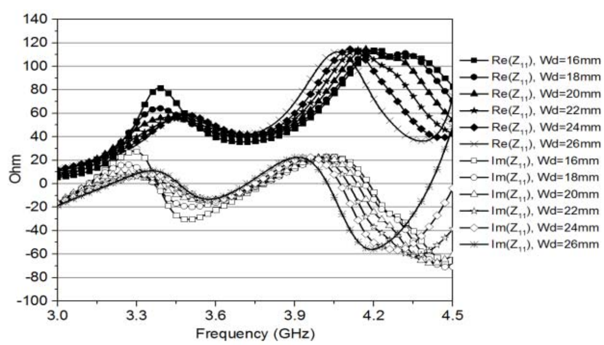

Fig. 12. Input impedance versus width of the dielectric resonator W_d.

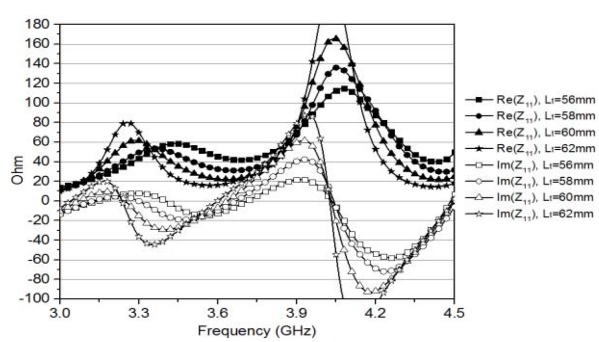

Fig. 13. Input impedance versus total length of the semi-loop L_t.

seen that the length of the slot plays a role of adjusting the matching condition and the operating bandwidth of the antenna. When the slot is short, the operational bandwidth is narrow, or other way around. Fig. 14(b) shows the simulated radiation patterns of the copolarization electric field in the E-plane with different sizes of the ground plane. Although the ground size changes from 100 mm × 100 mm ($1.15\lambda_o \times 1.15\lambda_o$) to 60 mm × 60 mm ($0.69\lambda_o \times 0.69\lambda_o$),

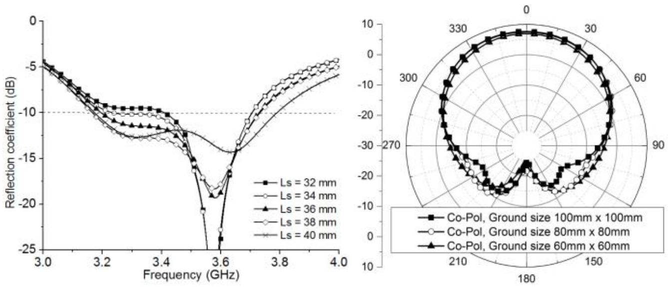

Fig. 14. (a) Simulated reflection coefficients versus the slot length L_s. (b) Simulated radiation patterns of copolarization in the E-plane with different sizes of the ground plane.

the back-lobe cancelation still works, which justifies that the working principle of the back-lobe cancelation.

B. Design Guideline

A proper design guideline is given as follows. Assume the free-space wavelength of the center frequency f_o is λ_o and the operating bandwidth spans from f_{lower} to f_{upper}.

Step 1—Determine the Length of the Semi-loop: The total length of the semi-loop can be selected slightly larger than $0.5\lambda_o$.

Step 2—Determine the Dimensions of the Dielectric Resonator: First, the resonant frequency f_d of a dielectric resonator can be determined by the eigenmode calculator of an EM simulator. The corresponding dimensions of the dielectric resonator can be used as a good starting point. Since the dimension of dielectric resonator controls the upper resonance of the antenna, the final value of f_d is usually larger than f_{upper}. Then, duplicating the semi-loop and the rectangular dielectric resonator in the orthogonal direction.

Step 3—Final Tuning: To achieve the back-lobe cancelation, a fine tuning of dimensions of the semi-loop and the dielectric resonator needs to be applied to achieve the best performance of matching and back-lobe cancelation in the operating frequency band.

V. Conclusion

A novel wideband ±45° dual-polarized MLDR-ME dipole antenna with low backward radiation is proposed. The proposed antenna structure is a legitimate combination of DRAs and metal semi-loop antennas. Two orthogonal dielectric bars support two orthogonal electric dipoles above the ground whereas the two orthogonal metal semi-loops can be equivalent to two orthogonal magnetic dipoles above the ground. As a result, each antenna port excites a pair of orthogonal electric and magnetic dipoles. With an appropriate design of the two types of dipoles, two resonances can be created in the operating frequency band and the backward radiation from the two types of orthogonal dipoles cancel each other, resulting in a wideband compact antenna with low backward radiation. A prototype antenna is designed, manufactured, and fully measured to validate the proposed antenna configuration. The ceramic prototype antenna can achieve a bandwidth of 11.4% for reflection coefficient lower than −15 dB and the peak gain of more than 7 dBi. The prototype antenna is very compact with electrical dimensions of $0.33\lambda_o \times 0.33\lambda_o \times 0.21\lambda_o$ with a high F/B ratio. With the attractive features of simplicity in structure, compactness in size, wide frequency band, and low backward radiation, the proposed antenna can find many applications in M-MIMO array antennas for future wireless systems.

Acknowledgment

The authors would like to thank Y. Hu of Jiaxing Glead Electronics Company, Ltd., for providing the ceramic samples and the reviewers for their valuable comments.

References

[1] R. Gabriel and M. Gottl, "Dual-polarized dipole antenna," U.S. Patent 6 313 809, Nov. 2001.

[2] M. Stolle and A. Scheyer, "Antenna having at least one dipole or an antenna element arrangement which is similar to a dipole," U.S. Patent 6 933 906, Aug. 2005.

[3] F. Rusek and *et al.*, "Scaling up MIMO: Opportunities and challenges with very large arrays," *IEEE Signal Process. Mag.*, vol. 30, no. 1, pp. 40–60, Jan. 2013.

[4] K.-L. Wu, C. Wei, X. Mei, and Z.-Y. Zhang, "Array-antenna decoupling surface," *IEEE Trans. Antennas Propag.*, vol. 65, no. 12, pp. 6728–6738, Dec. 2017.

[5] B. Li, C.-X. Hao, and X.-Q. Sheng, "A dual-mode quadrature-fed wideband circularly polarized dielectric resonator antenna," *IEEE Antennas Wireless Propag. Lett.*, vol. 8, pp. 1036–1038, Aug. 2009.

[6] X. S. Fang and K. W. Leung, "Designs of single-, dual-, wide-band rectangular dielectric resonator antennas," *IEEE Trans. Antennas Propag.*, vol. 59, no. 6, pp. 2409–2414, Jun. 2011.

[7] Y. Gao, Z. Feng, and L. Zhang, "Compact asymmetrical T-shaped dielectric resonator antenna for broadband applications," *IEEE Trans. Antennas Propag.*, vol. 60, no. 3, pp. 1611–1615, Mar. 2012.

[8] Y. X. Sun and K. W. Leung, "Dual-band and wideband dual-polarized cylindrical dielectric resonator antennas," *IEEE Antennas Wireless Propag. Lett.*, vol. 12, pp. 384–387, 2013.

[9] H. Tang, J.-X. Chen, W.-W. Yang, L.-H. Zhou, and W. Li, "Differential dual-band dual-polarized dielectric resonator antenna," *IEEE Trans. Antennas Propag.*, vol. 65, no. 2, pp. 855–860, Feb. 2017.

[10] K. W. Leung, E. H. Lim, and X. S. Fang, "Dielectric resonator antennas: From the basic to the aesthetic," *Proc. IEEE*, vol. 100, no. 7, pp. 2181–2193, Jul. 2012.

[11] S. K. Menon, B. Lethakumary, P. Mohanan, P. V. Bijumon, and M. T. Sebastian, "Wideband cylindrical dielectric resonator antenna excited using an L-strip feed," *Microw. Opt. Technol. Lett.*, vol. 42, no. 4, pp. 293–294, Aug. 2004.

[12] K. W. Leung, W. C. Wong, K. M. Luk, and E. K. N. Yung, "Annular slot-coupled dielectric resonator antenna," *Electron. Lett.*, vol. 34, no. 13, pp. 1275–1277, Jun. 1998.

[13] Y.-X. Guo and K.-M. Luk, "Dual-polarized dielectric resonator antennas," *IEEE Trans. Antennas Propag.*, vol. 51, no. 5, pp. 1120–1124, May 2003.

[14] C.-Y. Huang, J.-Y. Wu, and K.-L. Wong, "Cross-slot-coupled microstrip antenna and dielectric resonator antenna for circular polarization," *IEEE Trans. Antennas Propag.*, vol. 47, no. 4, pp. 605–609, Apr. 1999.

[15] K.-M. Luk and H. Wong, "A new wideband unidirectional antenna element," *Int. J. Microw. Opt. Technol.*, vol. 1, no. 1, pp. 35–44, Jun. 2006.

[16] L. Siu, H. Wong, and K. M. Luk, "A dual-polarized magneto-electric dipole with dielectric loading," *IEEE Trans. Antennas Propag.*, vol. 57, no. 3, pp. 616–623, Mar. 2009.

[17] L. Ge and K.-M. Luk, "A low-profile magneto-electric dipole antenna," *IEEE Trans. Antennas Propag.*, vol. 60, no. 4, pp. 1684–1689, Apr. 2012.

[18] M. Li and K. Luk, "A differential-fed magneto-electric dipole antenna for UWB applications," *IEEE Trans. Antennas Propag.*, vol. 61, no. 1, pp. 92–99, Jan. 2013.

[19] B. Q. Wu and K. M. Luk, "A broadband dual-polarized magneto-electric dipole antenna with simple feeds," *IEEE Antennas Wireless Propag. Lett.*, vol. 8, pp. 60–63, 2009.

[20] Q. Xue, S. W. Liao, and J. H. Xu, "A differentially-driven dual-polarized magneto-electric dipole antenna," *IEEE Trans. Antennas Propag.*, vol. 61, no. 1, pp. 425–430, Jan. 2013.

[21] Z. L. Ma and C. H. Chan, "Waveguide-based differentially fed dual-polarized magnetoelectric dipole antennas," *IEEE Trans. Antennas Propag.*, vol. 65, no. 8, pp. 3849–3857, Aug. 2017.

[22] L. Guo and K. W. Leung, "Compact linearly and circularly polarized unidirectional dielectric resonator antennas," *IEEE Trans. Antennas Propag.*, vol. 64, no. 6, pp. 2067–2074, Jun. 2016.

[23] Y.-M. Pan, K. W. Leung, and K. Lu, "Compact quasi-isotropic dielectric resonator antenna with small ground plane," *IEEE Trans. Antennas Propag.*, vol. 62, no. 2, pp. 577–585, Nov. 2013.

[24] D.-L. Wen, D.-Z. Dong, and Q.-X. Chu, "A wideband differentially fed dual-polarized antenna with stable radiation pattern for base stations," *IEEE Trans. Antennas Propag.*, vol. 65, no. 5, pp. 2248–2255, May 2017.

[25] Y. Gou, S. Yang, J. Li, and Z. Nie, "A compact dual-polarized printed dipole antenna with high isolation for wideband base station applications," *IEEE Trans. Antennas Propag.*, vol. 62, no. 8, pp. 4392–4395, Aug. 2014.